Soft Matter

PAPER

View Article Online
View Journal | View Issue

Cite this: *Soft Matter*, 2019, **15**, 477

Emergent topological phenomena in active polymeric fluids†

Raj Kumar Manna [a] and P. B. Sunil Kumar *[ab]

Polymeric fluids show a wealth of topological phenomena, from entanglement and reptation at microscales to orientational ordering and defect production at macroscales, which can be explained by statistical-mechanical theories. In the presence of activity, the latter must be augmented by forces that cause spontaneous chain motion and fluid flow. Here, using such augmented Langevin equations, we study active polymeric solutions and melts composed of chains of hydrodynamically interacting stresslets. In a spherical volume, contractile chains are unstable and self-knot into entangled melts at both low and high densities. Extensile chains in the same geometry form an unentangled reptating state at low densities and an entangled, coherently moving, non-reptating state at high densities. On a spherical surface, contractile chains show transitions, with increasing areal density, between isotropic, orientationally ordered and micro-phase separated states. Extensile chains in the same geometry show a transition between isotropic and nematic states. In both cases, defects in orientationally ordered states are produced athermally and without conserving topological charge. Our work reproduces the phenomenology of several recent experiments, highlights the importance of hydrodynamic interactions in active polymer fluids, and suggests non-equilibrium kinetic routes to topological structures that are otherwise difficult to obtain in equilibrium.

Received 28th September 2018,
Accepted 6th December 2018

DOI: 10.1039/c8sm01981a

rsc.li/soft-matter-journal

1 Introduction

The fluid states of long polymeric molecules are distinguished from their low-molecular weight counterparts by a fascinating variety of topological phenomena.[1–4] They arise from the collective properties of many polymer chains and, qualitatively, are largely insensitive to the microscopic properties of the constituents. All polymeric fluids, for instance, contain entanglements between chains and relax strains by reptation, a diffusive snaking motion of chains.[5] While these phenomena are confined to length scales comparable to the chain size, at larger length scales, emergent phenomena associated with the breaking of continuous symmetries make their appearance.[6,7] With the increase in density, polymeric fluids exhibit phase transitions from a disordered isotropic phase to orientationally ordered liquid-crystalline phases.[8,9] In addition to the usual disclinations – topological defects associated with the spontaneous breaking of rotational symmetry – polymeric liquid crystalline phases contain hairpins and chain ends, two classes of defects that can only exist in a phase of chains.[10–12] To understand how these topological phenomena determine the macroscopic properties of polymeric fluids has been one of the central goals of polymer science.[13,14]

For phenomena in or close to thermal equilibrium, statistical-mechanical theories, in which mechanical equations of motion are augmented by fluctuating forces of thermal origin, have been impressively successful in rationalizing experimental observations.[2,15] Recently, a new class of strongly non-equilibrium polymeric fluids have been synthesized in which ballistic polymeric motion can occur in the absence of external forces.[16–20] The assemblies of these "active" polymeric fluids have been shown to display large scale patterns such as lattices of asters and vortices,[16,21,22] swarm-like moving clusters and spirals,[23] and motile topological defects.[17,18,24] To understand these emergent structures,[25] in a collection of active polymers, many theoretical studies based on continuum- and particle-based models have been developed.[26–33] These active polymers contain mechanisms by which energy, drawn from internal or external reservoirs, is converted into mechanical work. This net flow of energy is dissipated in the ambient fluid to produce non-equilibrium steady states. The local conservation of momentum in the fluid implies that the activity-induced motion of chain segments can be transmitted through the fluid to other segments. This non-local coupling of spontaneous chain motion is a phenomenon without any equilibrium analogue. The novel emergent topological phenomena in such "active"

[a] Department of Physics, Indian Institute of Technology Madras, Chennai, India. E-mail: raj@physics.iitm.ac.in
[b] Department of Physics, Indian Institute of Technology Palakkad, Palakkad 678557, India. E-mail: sunil@iitpkd.ac.in

† Electronic supplementary information (ESI) available. See DOI: 10.1039/c8sm01981a

polymeric fluids cannot be understood within the framework of conventional statistical-mechanical theories, as they do not include the active forces that cause spontaneous chain motion.

Motivated by this lacuna, here we construct a statistical mechanical model of active polymeric fluids that takes into account both the spontaneous motion of chains and hydrodynamically mediated dissipative, long-ranged, many-body active forces that cause such motion. The model is framed in terms of Langevin equations, describing the motion of each polymer chain, which contains, in an explicit form, both intra-chain and inter-chain active forces.[34,35] Each active polymer is modeled as a chain of active beads connected by potentials that enforce linear connectivity, self-avoidance, and semi-flexibility.[36] The activity of each bead is represented by a stresslet, with magnitude S and the principal axis $\hat{\mathbf{t}}$, oriented along the local chain tangent. The beads produce extensile (contractile) flows along the principal axis for positive (negative) values of S. The forces between beads have contributions from their passive motion and their activity, which are described quantitatively by generalized Stokes laws.[35] Additionally, each bead experiences a confining potential that restricts it to either the surface or the interior of a closed manifold. Chain motion results from the balance of active forces, Stokes drag in the fluid, the constraining effect of the various potentials, and thermal fluctuations.

The key dimensionless parameter in the model is the activity number $\mathcal{A} = LS/\kappa$, where L is the chain length and κ is the chain bending rigidity.[36] It is the ratio of characteristic times $\tau_\kappa = \eta L^4/\kappa$ to $\tau_S = \eta L^3/S$, associated with chain elasticity and spontaneous flow, respectively, in a Stokesian fluid of viscosity η. The dynamics of a single chain has been studied extensively within this model to reveal curvature instabilities,[36] biomimetic oscillations,[37,38] and active stiffening.[39]

Here we study a collection of such chains comprising an active polymeric fluid, confined to the interior of a spherical volume or to the (permeable) surface bounding it. The first geometry can be realised in optical traps, while the second geometry is motivated by recent experiments on mixtures of bio-filaments and motor proteins confined to the interface of an emulsion droplet.[18] While the second geometry has been studied extensively[40–42] in the context of 2d active nematics, relatively few studies[37,38,45] explored the effect of activity induced bulk flows on the dynamics of active polymers. The key parameters are the chain density, quantified by volume (ϕ_v) and surface (ϕ_s) fractions, and the activity number $\mathcal{A}$. We simulate dilute solutions and melts of both contractile ($\mathcal{A} < 0$) and extensile ($\mathcal{A} > 0$) chains. Our results, summarised in Table 1, are partitioned into four combinations corresponding to volume or surface confinement and contractile or extensile activity. Contractile solutions in volume confinement are topologically unstable and yield self-knotted, entangled melts. Extensile chains in the same geometry form an unentangled reptating state at low densities and an entangled, coherently moving, non-reptating state at high densities. Contractile chains confined to a spherical surface show transitions between isotropic, orientationally ordered and microphase separated states. Extensile chains in the same geometry show a transition between isotropic and nematic states. In both cases, defects in ordered states are produced athermally and without the conservation of topological charge.

2 Method

We consider N_p active polymers confined to the surface or interior of a spherical volume. An active polymer is modeled as a chain of N_c spherical active beads of radius b, with the center of mass coordinate $\mathbf{R}_n$, and linear velocity $\mathbf{V}_n$. The total number of beads in the system is $N = N_p \times N_c$ and $n = 1, 2, \ldots, N$. The activity of the bead is represented by surface slip, truncated to the first non-trivial contribution, which is the stresslet. This is represented by a second-rank symmetric tensor

$$\mathbf{S}_n = S\left(\hat{\mathbf{t}}_n\hat{\mathbf{t}}_n - \frac{1}{3}\boldsymbol{\delta}\right)$$

which represents an apolar and achiral active bead. The equation of motion of a collection of such beads is[36,37,39]

$$\dot{\mathbf{R}}_n = \underbrace{\boldsymbol{\mu}^{\mathrm{TT}}_{nm}(\mathbf{R}_n,\mathbf{R}_m)\cdot\mathbf{F}^b_m}_{\text{passive}} + \underbrace{\boldsymbol{\pi}^{(\mathrm{TS})}_{nm}(\mathbf{R}_n,\mathbf{R}_m)\cdot\mathbf{S}_m}_{\text{active}} + \underbrace{\boldsymbol{\xi}_n}_{\text{Brownian}} \qquad (1)$$

where the mobility, $\boldsymbol{\mu}_{nm}$, and the propulsion, $\boldsymbol{\pi}_{nm}$, matrices are

$$\boldsymbol{\mu}^{\mathrm{TT}}_{nm}(\mathbf{R}_n,\mathbf{R}_m) = \mathcal{F}^0_n\mathcal{F}^0_m\mathbf{G}(\mathbf{R}_n,\mathbf{R}_m),$$

$$\boldsymbol{\pi}^{(\mathrm{TS})}_{nm}(\mathbf{R}_n,\mathbf{R}_m) = \mathcal{F}^0_n\mathcal{F}^1_m\boldsymbol{\nabla}_m\mathbf{G}(\mathbf{R}_n,\mathbf{R}_m),$$

$\mathbf{G}(\mathbf{r},\mathbf{r}')$ is Green's function of Stokes flow, and $\boldsymbol{\xi}_n$ is a noise that respects the fluctuation–dissipation relation. Here we take

$$8\pi\eta G_{ij}(\mathbf{r},\mathbf{r}') = \frac{\delta_{ij}}{\rho} + \frac{\rho_i\rho_j}{\rho^3},$$

with $\rho = \mathbf{r} - \mathbf{r}'$, to be the Oseen tensor. Finite-size corrections are encoded in the Faxen operator $\mathcal{F}^l_n = \left(1 + \frac{b^2}{4l+6}\boldsymbol{\nabla}^2\right)$. The principal axis $\hat{\mathbf{t}}_n$ of the stresslet is identified with the chain tangent. Here, we assume that the relative strength of the activity is so large that the Brownian noise makes negligible contribution to the dynamics. Thus, we neglect the effect of thermal fluctuations and work in the deterministic limit of the above dynamics.

The body force $\mathbf{F}^b_n$ on the n-th active bead is the gradient of the total potential,

$$\mathbf{F}^b_n = -\boldsymbol{\nabla}U.$$

Table 1 Summary of main results for contractile and extensile polymeric fluids in volume or surface confinement

	Contractile	Extensile
Volume confinement	Self-entanglement, stable entangled states	Mutual entanglement, entanglement transition
Surface confinement	T-Junctions, +1 defects, hairpins	I–N transition, $\pm\frac{1}{2}$ defects, hairpins

Here the potential U is the sum of the intra-polymer potential $U^{\alpha\alpha}$ and inter-polymer potential $U^{\alpha\beta}$, $U = \sum_{\alpha}\left(U^{\alpha\alpha} + \sum_{\beta>\alpha} U^{\alpha\beta}\right)$, where the indices α and β label the polymers. The intra-polymer potential consists of connectivity, semi-flexibility, self-avoidance and confining potentials,

$$U^{\alpha\alpha} = \sum_{m=1}^{N_c-1} U^{C}(\mathbf{R}_m, \mathbf{R}_{m+1}) + \sum_{m=2}^{N_c-2} U^{E}(\mathbf{R}_{m-1}, \mathbf{R}_m, \mathbf{R}_{m+1}) + \sum_{m<n} U^{S}(\mathbf{R}_m, \mathbf{R}_n) + \sum_{m=1}^{N_c} U^{Conf}(\mathbf{R}_m)$$

The connectivity potential is the two body harmonic spring potential $U^{C} = \frac{1}{2}k(|\mathbf{R}_m - \mathbf{R}_{m+1}| - b_0)^2$, where b_0 and k is the equilibrium bond length and elasticity parameter respectively. The elastic potential $U^{E} = \bar{\kappa}(1 - \cos\phi)$ penalizes departures of the angle ϕ between consecutive bond vectors from its equilibrium value of zero. The rigidity parameter $\bar{\kappa}$ is related to the chain bending rigidity as $\kappa = b_0\bar{\kappa}$. The self-avoidance potential U^{S} is taken as the Weeks–Chandler–Andersen potential, which vanishes if the distance between beads $r_{mn} = |\mathbf{R}_m - \mathbf{R}_n|$ exceeds $2b$. In addition, active polymers are subjected to a potential which confines the polymers to the interior of a spherical volume or on a spherical surface. For the volume confinement, the confining potential is given by

$$U^{Conf}(\mathbf{R}_n) = \begin{cases} c\dfrac{\exp(1/(R-r))}{(l_{max}-r)} & r > R, \quad r < l_{min} \\ 0 & \text{Otherwise} \end{cases} \tag{2}$$

and the potential that confines the polymers on the surface of a sphere is taken as

$$U^{Conf}(\mathbf{R}_n) = \begin{cases} c\dfrac{\exp(1/(r-R))}{(r-l_{min})} & r < R, \quad r > l_{min} \\ c\dfrac{\exp(1/(R-r))}{(l_{max}-r)} & r > R, \quad r < l_{max} \\ 0 & r = R \end{cases}$$

where R is the radius of the confining sphere, $r = |\mathbf{R}_n|$, $l_{min} = R - 4b$, and $l_{max} = R + 4b$. This confining potential is applied only to polymers and the fluid flow is infinite. The inter-polymer potential $U^{\alpha\beta}$ consists of the self-avoidance term alone.

The position of each active bead changes according to the kinematic equation $\dot{\mathbf{R}}_n = \mathbf{V}_n$. We use an Euler scheme to integrate the equation of motion. A complete list of parameters used in the simulations is given in Table S1 of the ESI.†

3 Active fluid flows

It has been shown in earlier simulations[36,39] that active fluid flows, in an unbounded geometry, suppress transverse perturbations in a contractile active polymer and enhance it in an extensile active polymer. In the case of a single active filament, this nature of active fluid flows leads to stabilising the straight conformation of a contractile active polymer and propulsion of a bend extensile active polymer in the direction opposite to its signed curvature.[36,39] Similar behaviour is also observed when the polymer is confined to a surface of a sphere, with a contractile polymer stable in the linear configuration and an extensile polymer spontaneously moving opposite to the direction of its signed curvature (see Fig. S1 and Movie S1, ESI†). However, the dynamics of the polymers and its coupling with the fluid flows become more interesting with increasing number of polymers. Fig. 1 shows the dynamics of a pair of contractile (top panels) and extensile polymers (bottom panels) on the surface of a sphere, together with the fluid flows projected onto the surface of the confining sphere. The attractive flows at the polymer end drive contractile polymers to form T-junctions (Fig. 1(c) and Movie S1, ESI†), similar to that observed in the case of contractile stiff rods in two dimensions.[43] On the other hand, fluid flows around extensile polymers, being in a direction opposite to that of contractile polymers, lead to repulsion of their ends, lateral attraction, and spontaneous motion polymers (Fig. 1(d–f) and Movie S1, ESI†).

We turn now to our results.

4 Knots, reptation, entanglement

4.1 Contractile activity and volume confinement

Our first result, shown in the top panels of Fig. 2, is on the dynamics of a pair of contractile polymers confined to a spherical volume whose diameter, $2R$, is smaller than the chain length, L. Under the influence of their mutual hydrodynamic flow, a pair of initially separated chains pass through a transient state with an increasing number of knots and links to reach a stable entangled state with a constant number of knots and links. Instantaneous measures of the degrees of knotting and linking are provided by the crossing, Cn, and linking, Ln, numbers respectively (see the ESI†). We compute their averages through the course of the dynamics, as shown in Fig. 2d and Movie S2 (ESI†). From the dynamics of pairs, it is clear that the initial configuration of separated chains at any volume fraction is unstable and flows into a stable entangled state. This is confirmed by simulations for volume fractions φ_v = 0.08, 0.16, 0.20, and 0.23, shown in Fig. 2(e and f) and Movie S2 (ESI†). For confinement diameters that are larger than L, initially separated chains do not knot or link. This is because, in an unbounded geometry, hydrodynamic flows produced by a contractile polymer suppress its transverse perturbation and a straight conformation is stable.[39] Therefore, at low volume concentration, in the absence of strong confinement (for $2R > L$), contractile polymers are always in the straight conformation (see Fig. S3, ESI†). However, an entangled state emerges, with a gradual increase in the volume fraction, which is qualitatively the same as the entangled state for $2R < L$. These results are illustrated in Fig. S3 (ESI†).

4.2 Extensile activity and volume confinement

Extensile activity completely alters the dynamics seen above. At low volume concentration, for $2R < L$, chains move ballistically

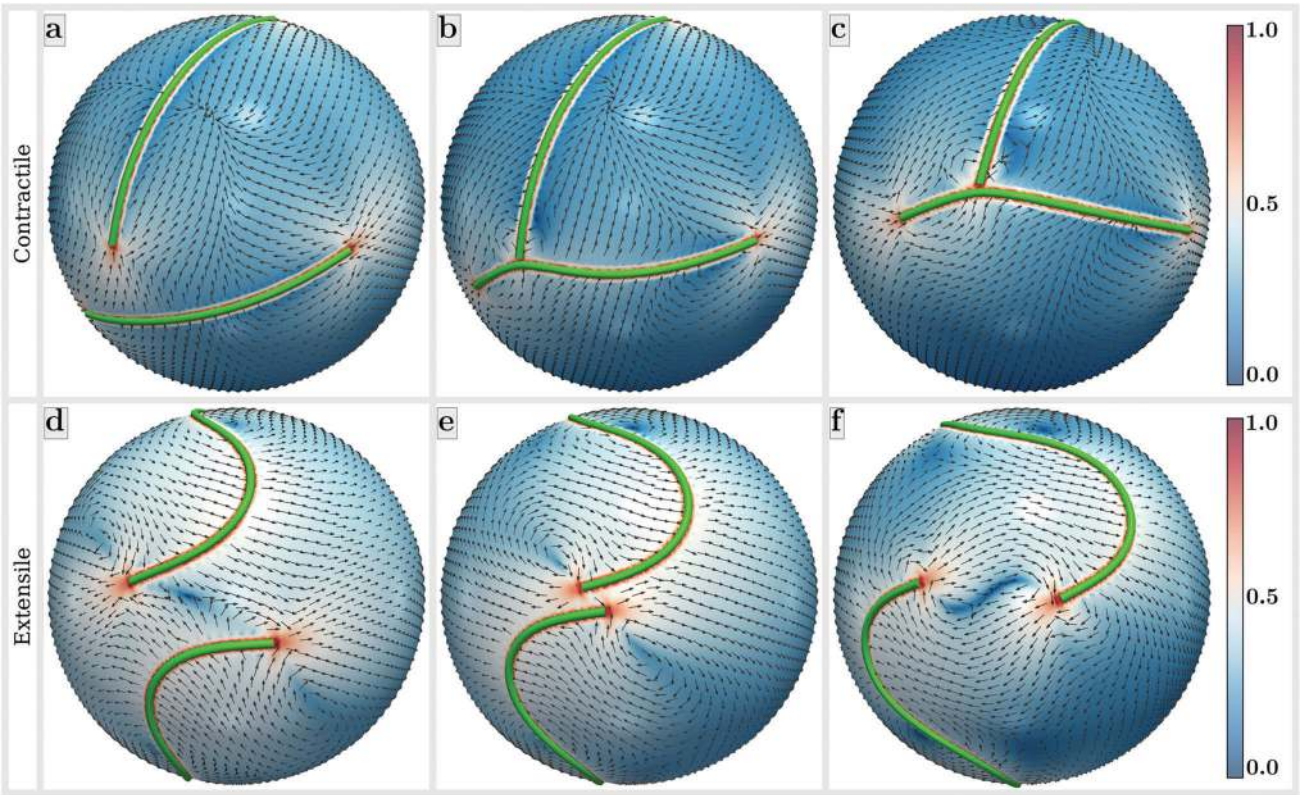

Fig. 1 Fluid flows produced by a pair of contractile (top panels) and extensile polymers (bottom panels) on the surface of a sphere. For clarity, only the fluid flow at the surface is shown. The first three panels (a–c) show that attractive flows at the end of the contractile polymers lead to the formation of T-junctions. Fluid flows around the extensile polymers (d–f) enhance any transverse perturbation, which generates spontaneous motion of individual polymers. Arrows represent the direction of fluid flows projected onto the surface of the confining sphere. Colors indicate the logarithm of the magnitude of fluid velocity normalised by its maximum. The activity numbers, $\mathcal{A}$, for the top and the bottom panels are -30 and 30 respectively.

within the confining volume and do not knot or link. With an increase in volume fraction, the chains begin to align parallel to each other. At low values of activity, chains move collectively but additionally slide past each other. Unlike reptation, where the distance between chain centroids grows diffusively, here their distance grows ballistically. We call this motion "active reptation". With the increase in activity, chains confine into a bundle and the bundle rotates as a single rigid body. These results are illustrated in Fig. 3(a–d) and Movie S3 (ESI†). Some chains are coloured blue as a guide to the eye.

To quantify the integrity of the bundle, we compute the auto-correlation, $C(\tau) = \langle r_{ij}^{\alpha\beta}(t) r_{ij}^{\alpha\beta}(t+\tau)\rangle$, of the distance, $r_{ij}^{\alpha\beta} = |\mathbf{r}_i^{\alpha} - \mathrm{r}_j^{\beta}|$, between monomer i on chain α and monomer j on chain β, summing over all monomers and chains. The enhanced correlation with an increase in activity reflects the transition from an incoherent motion, where reptation dominates, to a coherent motion, where reptation is largely absent. The auto-correlation is well-approximated by an exponential, $C(\tau) = c\exp[-\tau/\tau_c]$, for all chosen values of activity. The relaxation time, τ_c, increases monotonically with volume fraction, due to the enhanced steric constraints (Fig. 3f). On the other hand, with activity it initially decreases as active reptation is able to relax configurations and then begins to increase as coherent motion sets in (Fig. 3g). The minimum in τ_c, as a function of activity, marks the onset of coherent motion. A state diagram in the activity number–volume fraction plane summarises the results of 72 parameter values, confirming that the entangled state emerges at high activity and large volume fraction values (Fig. 3h). The natures of this transition, viewed from either the dynamical system or thermodynamic point of view, remain to be explored.

Entangled states. As is evident in the snapshots, the nature of the entangled states of extensile polymers is different from that formed by contractile active polymers. This difference between the entangled states of extensile and contractile polymers is obvious from the average crossing number $\langle Cn\rangle$ and the average linking number $\langle Ln\rangle$, which are the measures of self- and inter-chain entanglement respectively (see Fig. S2 and S5, ESI†). The average linking number $\langle Ln\rangle$ of extensile polymers is much lower than that of contractile polymers, implying that the inter-chain entanglement is lower for extensile polymers. On the other hand, the crossing number $\langle Cn\rangle$, indicating the self-entanglement, is higher at high values of ϕ_v for extensile polymers. These results indicate that the collective motion of extensile polymers is through more localised linking involving many polymers, while a few polymers linking to many control the bundling of contractile polymers at higher densities.

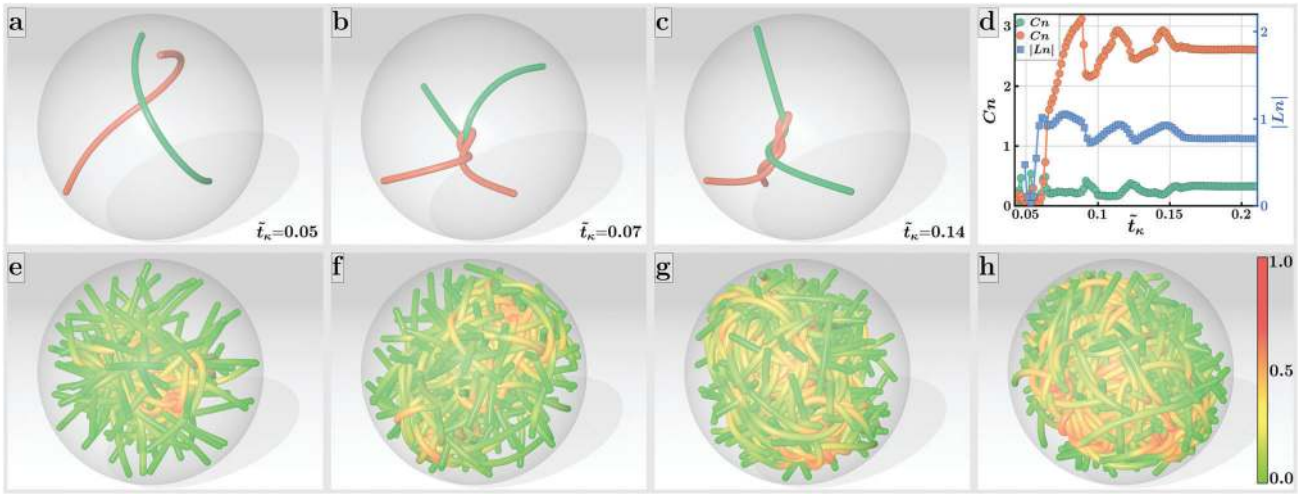

Fig. 2 Contractile active polymers in volume confinement, for confinement diameter less than chain length. The first three panels (a–c) show the activity-induced knotting and linking dynamics of a pair of chains. The corresponding variations along the dynamical trajectory of the instantaneous average crossing number, $Cn(t)$, and the absolute value of the average linking number, $|Ln(t)|$, are shown in scaled time $\tilde{t}_\kappa = t/\tau_\kappa$ in (d). This tendency of chain pairs to spontaneously entangle implies that dilute solutions of separated chains are always unstable in the disentangled states and lead, at any volume fraction ϕ_v, to stable entangled states. This is verified by simulations that produce entangled configurations at volume fractions ϕ_v = 0.08, 0.16, 0.20, and 0.23, shown in the remaining panels (e–h). For all the panels, the activity number $\mathcal{A}$ is −30. Each chain in the bottom panels is colored from green to red with increasing normalized magnitude of its local curvature.

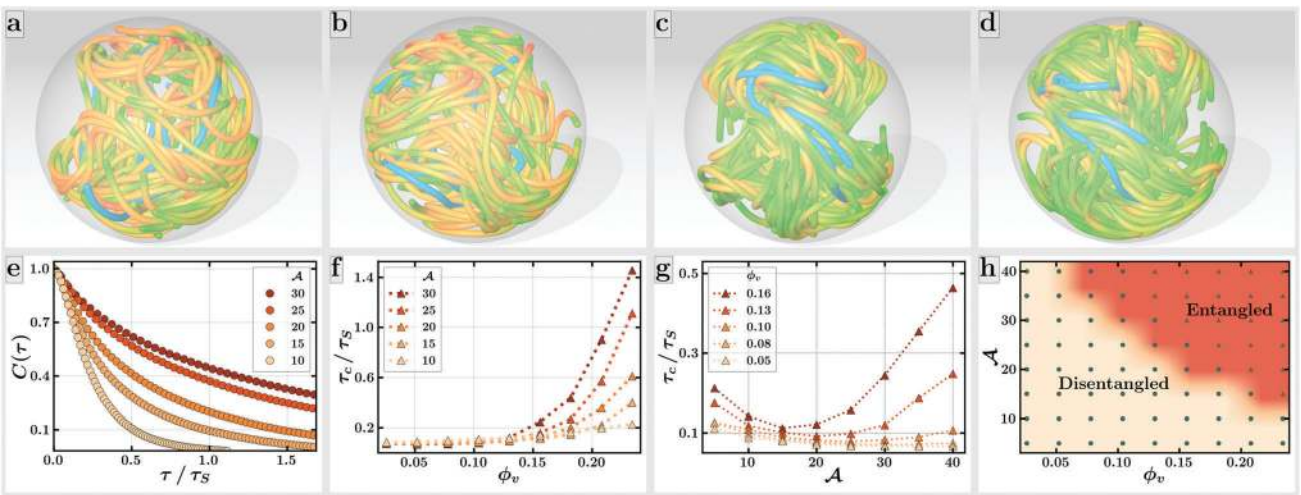

Fig. 3 Extensile active polymers in volume confinement, for confinement diameter less than chain length. The top panels show configurations at activity number $\mathcal{A} = 30$ and volume fraction ϕ_v = 0.10 (first two panels) and volume fraction ϕ_v = 0.23 (last two panels). Chains are in a disentangled, reptating state in (a and b) and in an entangled, coherently moving, non-reptating state in (c and d). Each chain is colored from green to red with increasing normalized magnitude of its local curvature using the same colorbar as in Fig. 2. Some chains are labelled blue as a guide to the eye. The bottom panels show quantitative measures of the transition from reptating to coherent motion. The enhancement of the autocorrelation, $C(\tau)$, of the distance between monomer pairs belonging to different polymers, plotted in units of the active relaxation time τ_S is shown in (e). This enhancement is quantified by plotting the characteristic time scale τ_c as a function of volume fraction for different activities in (f) and as a function of activity for different volume fractions in (g). The minimum in the $\tau_c(\mathcal{A})$ curve marks the onset of entanglement. This minimum is used to locate the boundary between unentangled and entangled states in the activity number–volume fraction plane in (h).

5 Order, elasticity, defects

When active polymers are confined to the surface of a manifold, the possibility of knots and links is precluded, as are the entangled states observed in volume confinement. Instead, it is now possible, by increasing the polymer surface fraction, ϕ_S, to transit from an isotropic state, in which the local chain tangents, viewed as a director, are orientationally disordered, to a nematic state, in which they are orientationally ordered. While such isotropic–nematic transitions have been well-studied in passive polymers both in the bulk and at surfaces, here, the presence of activity brings with it a number of surprising differences. We present the results of our simulations, sectioned, as before, into contractile and extensile activity.

5.1 Contractile activity and surface confinement

In two dimensions, two rigid extensile polymers attract sideways, forming parallel configurations, while two rigid contractile filaments align perpendicular to each other.[43] This basic difference between the preferred orientations of the contractile and extensile filaments also occurs in the configurations of semiflexible active filaments constrained to move in two dimensions. The configurations of contractile polymers on the surface of a sphere in the activity number–surface density plane are shown in Fig. 4 and Movie S4 (ESI†). The tendency of the filament ends to align perpendicular to the filament body, at moderate activity and surface fractions, leads to the formation of loops (+1 defects) and T junctions (+1/2 defects). The formation of T junctions is due to the attractive flows at the polymer ends (see Fig. 1 and Movie S1, ESI†). Similar T junctions are observed in the simulation of contractile stiff rods[43] and in the experiment with extensile gold–platinum–gold rods.[44] The number of these defects at any surface density increases as the activity increases (Fig. S6, ESI†). As can be seen from Fig. S6 of the ESI,† the rate of production of +1 defects also increases with activity. The contractile polymers suppress the formation of highly curved structures, and the loops are stabilised only by the T junctions at the polymer ends. At higher activity, wavy curvature instability appears along the polymers, the orientational order is lost and the contractile polymers form an isotropic phase (bottom panels of Fig. 4). This polymer crumpling is the result of compressive stress from the contractile flows. However, the validity of the assumption that the stresslets are aligned along the tangent to the polymer breaks down once the polymers form this crumpling state.

5.2 Extensile activity and surface confinement

At small surface fractions, extensile active polymers move disjointly on the surface of the sphere (Movie S5, ESI†). With increasing polymer surface fraction, hydrodynamic interactions between polymers becomes appreciable to align and cluster the polymers, leading to a nematic phase. We identify regions in

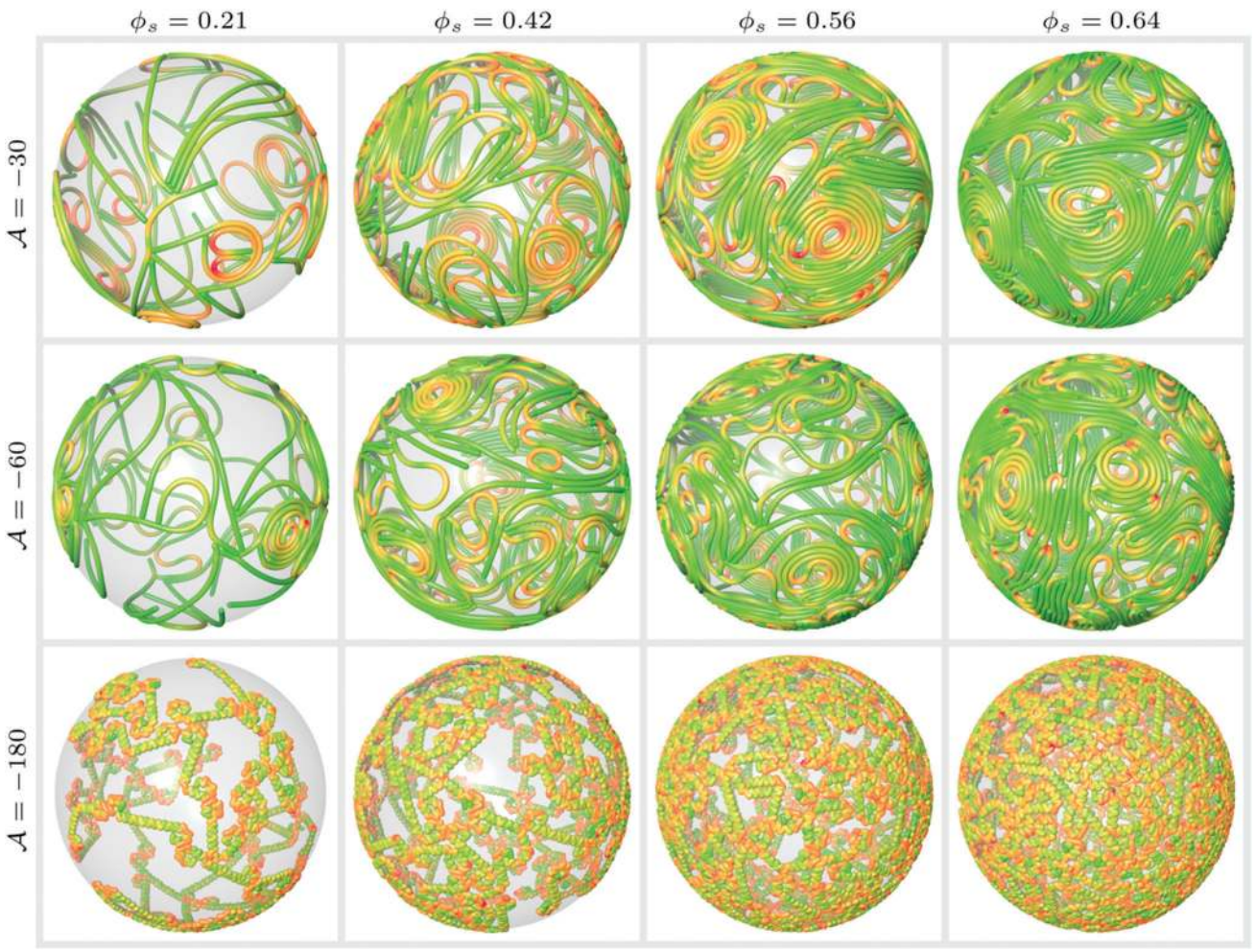

Fig. 4 Contractile active polymers in surface confinement. The 12 panels show instantaneous configurations for different values of surface fraction ϕ_s and activity $\mathcal{A}$. Starting with an isotropic phase on the top left, increases in the volume fraction produce an orientationally ordered phase dense with +1 disclinations, while increasing the activity leads to another isotropic phase in which the chains exhibit oscillatory curvature instability. Each chain is colored from green to red with increasing normalized magnitude of its local curvature using the same colorbar as in Fig. 2.

the parameter space of ϕ_s and $\mathcal{A}$ where these non-equilibrium nematic phases are stable (see Fig. 5).

In the nematic phase, the clusters of polymers generated are dynamic objects, with the collective motion of the polymers creating and annihilating +1/2 hairpin defects and −1/2 defects. Snapshots depicting the dynamics of active polymers on the surface of the sphere are shown in Fig. 6(a–d). There are several differences between the orientational field seen here and that in a conventional equilibrium liquid crystalline system, with the most important being the ability of individual polymers to self-propel, allowing for active relaxation of the system. The polymers move such that the curved regions on a polymer can slide along its length and the center of mass velocity of the polymer is proportional to and in the direction opposite to its total curvature.[36] The persistent collective motion of active polymers leads to the defects which are spontaneously created and annihilated (Movie S5, ESI†) at all times. Since polymers with higher curvature move more rapidly, the natural tendency is for high curvature polymers to accumulate behind those with lower curvature, forming the +1/2 defects shown in Fig. 6(a). For the same reason, these defects accumulate behind a straight segment, which is the slowest moving, forming a −1/2 defect, or have a vacant region in front of them. Defect annihilation dynamics is also quite different from that in equilibrium systems and is mainly through a process in which polymers actively slither past each other. Though this process is akin to reptation, the polymer motion is no longer diffusive but is ballistic and configurations can relax much more rapidly by this active reptation than they can be in equilibrium reptation. Another distinguishing feature of these defects is the different types of ±1/2 defects that are possible. There are two types of −1/2 defects – one in which the core is empty and the other in which the core is filled with polymer endings. Similarly, there are two types of +1/2 defects – a simple hairpin bend and the other in which the bend encloses line endings.

Defect dynamics. To quantify the creation and annihilation dynamics of defects created by extensile active polymers on the spherical surface, we calculate the number of hairpin defects by

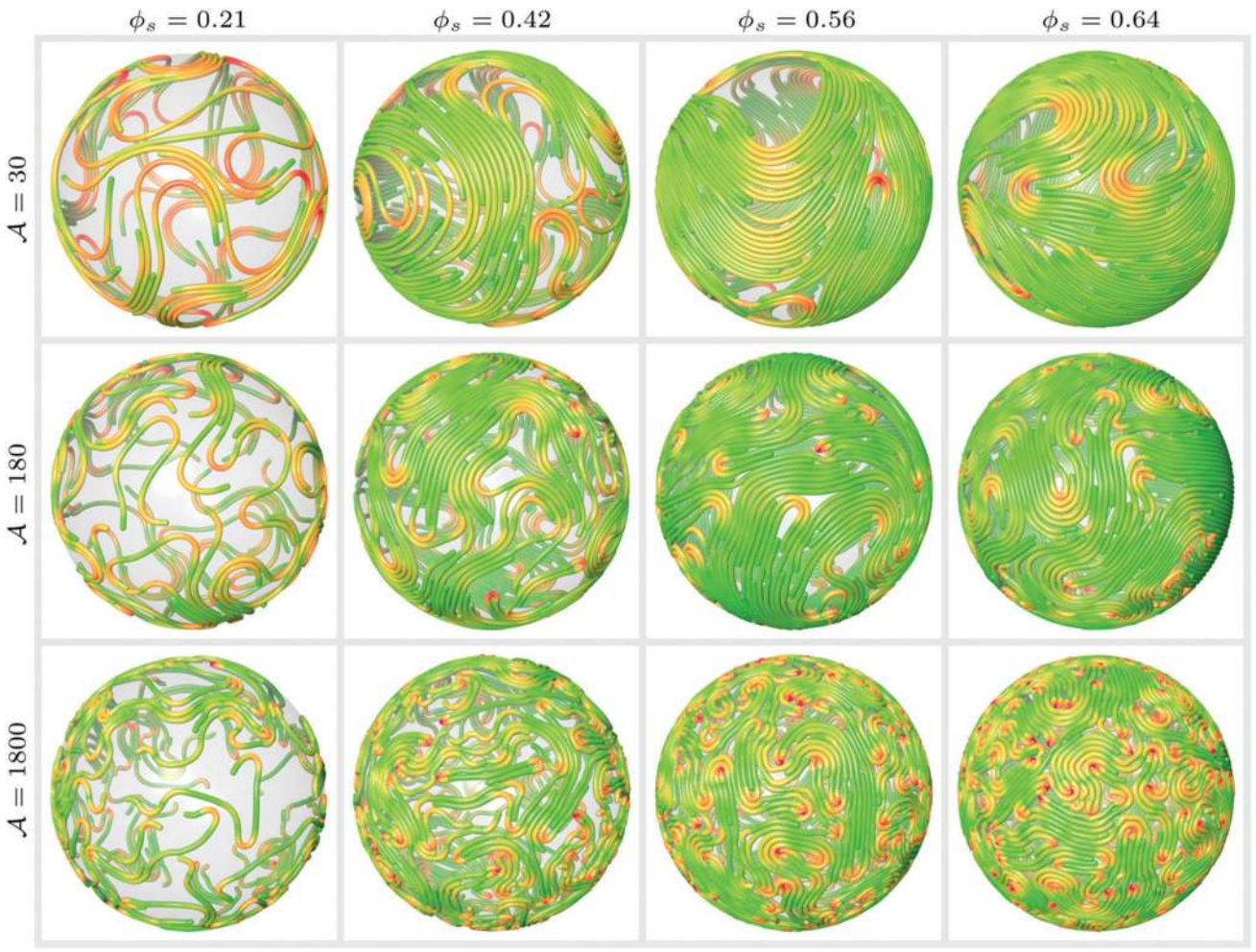

Fig. 5 Extensile active polymers in surface confinement. The 12 panels show instantaneous configurations for different values of surface fraction ϕ_s and activity $\mathcal{A}$. There is a clear signature of an athermal non-equilibrium isotropic–nematic transition as ϕ_s is increased and $\mathcal{A}$ is decreased. The nematic phase contains $\pm\frac{1}{2}$ disclinations, generic to any nematic phase and, specifically, chain ends and hairpins found only in liquid-crystalline polymers. Each chain is colored from green to red with increasing normalized magnitude of its local curvature using the same colorbar as in Fig. 2.

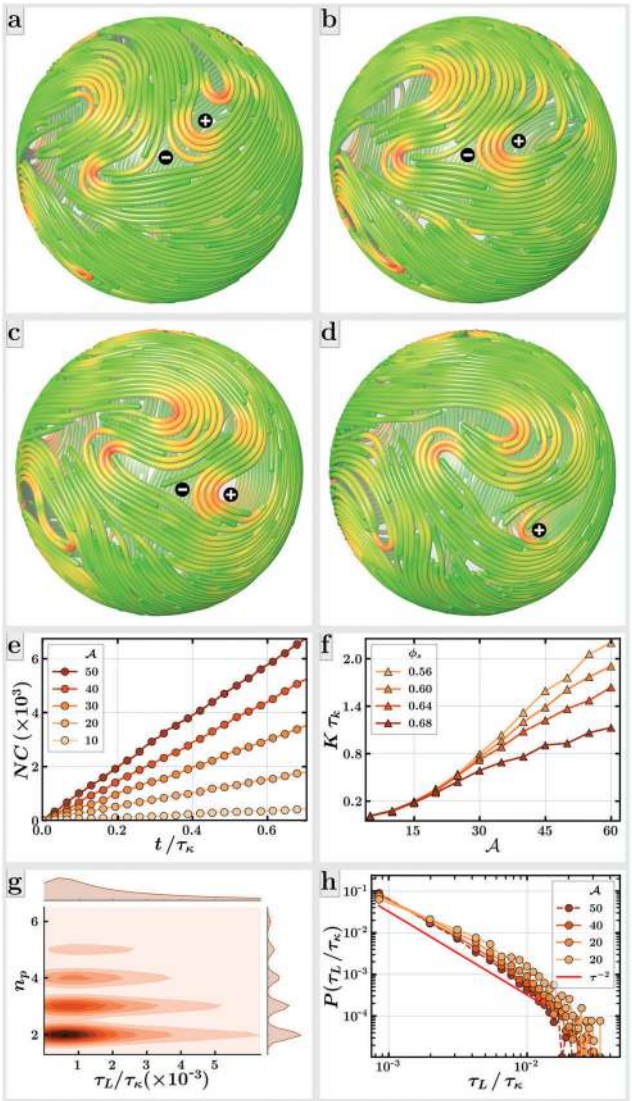

Fig. 6 Dynamics of disclinations in extensile surface-confined active polymers. The first four panels (a–d) show configurations along a dynamical trajectory with the $\pm\frac{1}{2}$ disclinations marked by the $\pm$ signs. Each chain is colored from green to red with increasing normalized magnitude of its local curvature using the same colorbar as in Fig. 2. The most distinctive feature of the dynamics is the non-conservation of topological charge where, as shown in (d), the $-\frac{1}{2}$ disclination disappears leaving an uncompensated $+\frac{1}{2}$ disclination. This is possible due to the finite energy cost of individual disclinations arising from the screening of splay. In (e) the total number of defects (including both disclinations and hairpins) produced up to time t is plotted for various activities, showing that the rate of defect production is constant and increases with activity. In (f), this rate, non-dimensionalised by τ_κ, is plotted as a function of activity for various surface fractions. Defect production is suppressed at high surface fractions due to the increased steric cost of bending. In (g), the joint distribution of the number of chains in a defect and its lifetime is shown. Defects with fewer chains have longer lifetimes. The marginal distribution of lifetimes is shown in (h). The red line is a guide to the eye. Simulations in the first four panels are for $\phi_s = 0.64$ and $\mathcal{A} = 30$.

tracking high curvature regions that are clustered together (see the ESI† for details on identification of defects). The total number of such defects created up to a time t as a function of t, for different values of activity, is shown in Fig. 6(e). The total number of defects annihilated up to a time t also increases with t in a similar fashion, leading to a steady state wherein the number of defects at any time fluctuates around a mean value (Fig. S7, ESI†). The dimensionless rate of defect production $K\tau_\kappa$, where K is the rate of production of defects and τ_κ is the bending relaxation time, as a function of activity for different polymer surface fractions is shown in Fig. 6(f). The rate of production of defects increases as the activity increases for all volume fraction values. There exists a critical activity above which we see a sharp increase in the rate of production of defects. This critical activity is independent of the surface fraction occupied by polymers and $\mathcal{A}_c \sim 15$. Since the possible number of defects is limited by the number of polymers, the defect production rate eventually slows down. Similarly, the velocity with which the polymer moves is smaller when the surface fraction occupied by the polymer is higher, which lowers the defect production rate. The above two factors are evident from Fig. 6(f).

In the regime where $\mathcal{A} \gg 1$ active relaxation dominates and the hairpins relax rapidly. However, for a +1/2 defect to relax, collective motion of many polymers is required. To understand how the number of filaments in a defect affects its lifetime τ_L, we plot the joint distribution of the lifetimes of defects and the associated number of polymers in Fig. 6(g) at a constant activity $\mathcal{A} = 30$. For a given surface fraction of polymers, the lifetimes of defects with more associated polymers are shorter as they have a higher active velocity, which accelerates active reptation of polymers, the main mechanism for the annihilation of defects. The defects with higher lifetimes have fewer polymers associated with them.

We compute the distribution of the lifetimes of defects for different values of activity at a constant volume fraction and see that they decay as an inverse square of time with an exponential cut off. This distribution for different values of activity at surface fraction $\phi_s = 0.64$ is shown in Fig. 6(h). We see from the figure that the lifetime of defects is smaller for higher activity, as expected from increased active reptation.

6 Conclusions

The collective dynamics of extensile and contractile active polymers have been studied through Brownian microhydrodynamics simulations, which take into account forces and torques mediated by active flow. The effects of activity and polymer density on the dynamics of active polymers confined to the surface or interior of a spherical volume have been investigated. The state formed by the contractile polymers in the volume confinement is found to depend on the diameter of the spherical volume to which they are confined. When the length of the polymer is larger than the confinement diameter, the chains show an entangled state at all densities. However, extensile active polymers subjected to the same confinement form an entangled, coherently moving state only above a critical volume fraction and activity. The critical activity itself

decreases as the volume fraction of the polymer increases. The nature of the entangled state in the extensile polymers is quite different from that in contractile polymers. This difference is brought out by the average polymer linking number and crossing number. Analysis of these numbers show that, in the case of contractile polymers, only a few filaments are responsible for entanglements.

When confined to move on the surface of a sphere, active polymers exhibit characteristic topological phenomena. Contractile polymers in surface confinement form loops (+1 defects) and T junctions irrespective of surface density and activity. In contrast, extensile polymers show orientationally ordered regions at the moderate activity and surface density of the polymer. Spontaneous and persistent collective motion of extensile active polymers in the ordered phase leads to the creation and annihilation of half-integer disclinations. The number of such defects can be controlled by the strength of activity. The important characteristic of the ordered states of both contractile and extensile cases is that topological charge is not conserved. This is because, unlike continuum theory, the ordered state of the chain resolved model presented here allows for empty spaces which makes isolated defect annihilation possible.

In the study presented here, it is assumed that the viscosities of fluids in the regions interior and exterior to the spherical region of confinement are the same and the fluid is allowed to flow freely through the boundary. It may be interesting to explore the effects of the different viscosities of the fluid in the inner and outer regions of confinement on the collective dynamics of active polymers. After this manuscript was submitted, a paper on the structure and dynamics of a single active polymer with no-slip boundary conditions on the confining sphere appeared in print.[45] The effects of such no-slip boundary conditions on the confining sphere can significantly change the dynamics of many active polymers. A systematic study of these aspects will be presented in the future.

Conflicts of interest

There are no conflicts to declare.

Acknowledgements

We gratefully acknowledge Prof. Ronojoy Adhikari for his suggestion to study active polymers in geometric confinement, many insightful discussions about active polymer systems, and critical comments on the presentation of this study. We would also like to thank Abhrajit Laskar, Rajesh Singh, and Sachin Krishnan for useful discussions. R. K. M. wishes to acknowledge the Abdus Salam International Center for Theoretical Physics (ICTP) for the kind invitation to the workshop on Knots and Links in Biological and Soft Matter Systems. Numerical simulations were performed at the High-Performance Computing Environment of IIT Madras and IIT Palakkad.

References

1 P.-G. De Gennes, *Scaling concepts in polymer physics*, Cornell University Press, 1979.
2 M. Doi and S. F. Edwards, *The theory of polymer dynamics*, Oxford University Press, 1988, vol. 73.
3 S. G. Whittington, W. De Sumners and T. Lodge, *Topology and geometry in polymer science*, Springer Science & Business Media, 2012, vol. 103.
4 A. L. Kholodenko and T. A. Vilgis, *Phys. Rep.*, 1998, **298**, 251–370.
5 P.-G. de Gennes, *J. Chem. Phys.*, 1971, **55**, 572–579.
6 L. Landau and E. Lifshitz, *Statistical Physics, Part 1: (Course of Theoretical Physics)*, 1980, vol. 5.
7 P. Chaikin and T. Lubensky, *Principles of Condensed Matter Physics*, Cambridge University Press, 2000.
8 A. M. Donald, A. H. Windle and S. Hanna, *Liquid crystalline polymers*, Cambridge University Press, 2006.
9 A. Nikoubashman, D. A. Vega, K. Binder and A. Milchev, *Phys. Rev. Lett.*, 2017, **118**, 217803.
10 M. Kleman, L. Liebert and L. Strzelecki, *Polymer*, 1983, **24**, 295–299.
11 G. Mazelet and M. Kleman, *Polymer*, 1986, **27**, 714–720.
12 J. V. Selinger and R. F. Bruinsma, *J. Phys. II*, 1992, **2**, 1215–1236.
13 R. B. Bird, R. C. Armstrong and O. Hassager, *Dynamics of polymeric liquids*, Fluid Mechanics, 1987, vol. 1.
14 R. B. Bird, R. C. Armstrong, O. Hassager and C. Curtiss, *Dynamics of Polymeric Liquids: Kinetic Theory*, 1987, vol. 2.
15 H. Yamakawa, *Modern theory of polymer solutions*, Harper & Row, 1971.
16 Y. Sumino, K. H. Nagai, Y. Shitaka, D. Tanaka, K. Yoshikawa, H. Chaté and K. Oiwa, *Nature*, 2012, **483**, 448–452.
17 T. Sanchez, D. T. Chen, S. J. DeCamp, M. Heymann and Z. Dogic, *Nature*, 2012, **491**, 431–434.
18 F. C. Keber, E. Loiseau, T. Sanchez, S. J. DeCamp, L. Giomi, M. J. Bowick, M. C. Marchetti, Z. Dogic and A. R. Bausch, *Science*, 2014, **345**, 1135–1139.
19 B. Biswas, R. K. Manna, A. Laskar, P. B. S. Kumar, R. Adhikari and G. Kumaraswamy, *ACS Nano*, 2017, **11**, 10025–10031.
20 S. J. DeCamp, G. S. Redner, A. Baskaran, M. F. Hagan and Z. Dogic, *Nat. Mater.*, 2015, **14**, 1110–1115.
21 T. Surrey, F. Nédélec, S. Leibler and E. Karsenti, *Science*, 2001, **292**, 1167–1171.
22 D. Saintillan and M. J. Shelley, *Phys. Rev. Lett.*, 2007, **99**, 058102.
23 V. Schaller, C. Weber, C. Semmrich, E. Frey and A. R. Bausch, *Nature*, 2010, **467**, 73–77.
24 P. Guillamat, J. Ignés-Mullol and F. Sagués, *Proc. Natl. Acad. Sci. U. S. A.*, 2016, **113**, 5498–5502.
25 F. Huber, J. Schnauß, S. Rönicke, P. Rauch, K. Müller, C. Fütterer and J. Käs, *Adv. Phys.*, 2013, **62**, 1–112.
26 D. Saintillan and M. J. Shelley, *J. R. Soc., Interface*, 2012, **9**, 571–585.

27 S. P. Thampi, R. Golestanian and J. M. Yeomans, *Phys. Rev. Lett.*, 2013, **111**, 118101.
28 D. Saintillan and M. J. Shelley, *Complex fluids in biological systems*, Springer, 2015, pp. 319–355.
29 R. G. Winkler, J. Elgeti and G. Gompper, *J. Phys. Soc. Jpn.*, 2017, **86**, 101014.
30 D. Khoromskaia and G. P. Alexander, *New J. Phys.*, 2017, **19**, 103043.
31 A. Doostmohammadi, J. Ignés-Mullol, J. M. Yeomans and F. Sagués, *Nat. Commun.*, 2018, **9**, 3246.
32 K. Prathyusha, S. Henkes and R. Sknepnek, *Phys. Rev. E*, 2018, **97**, 022606.
33 Ö. Duman, R. E. Isele-Holder, J. Elgeti and G. Gompper, *Soft Matter*, 2018, **14**, 4483–4494.
34 R. Singh and R. Adhikari, *Phys. Rev. Lett.*, 2016, **117**, 228002.
35 R. Singh and R. Adhikari, *J. Phys. Commun.*, 2018, **2**, 025025.
36 G. Jayaraman, S. Ramachandran, S. Ghose, A. Laskar, M. S. Bhamla, P. B. S. Kumar and R. Adhikari, *Phys. Rev. Lett.*, 2012, **109**, 158302.
37 A. Laskar, R. Singh, S. Ghose, G. Jayaraman, P. B. S. Kumar and R. Adhikari, *Sci. Rep.*, 2013, **3**, 1964.
38 R. K. Manna, P. B. S. Kumar and R. Adhikari, *J. Chem. Phys.*, 2017, **146**, 024901.
39 A. Laskar and R. Adhikari, *Soft Matter*, 2015, **11**, 9073–9085.
40 S. Henkes, M. C. Marchetti and R. Sknepnek, *Phys. Rev. E*, 2018, **97**, 042605.
41 R. Zhang, Y. Zhou, M. Rahimi and J. J. De Pablo, *Nat. Commun.*, 2016, **7**, 13483.
42 D. Khoromskaia and G. P. Alexander, *Phys. Rev. E: Stat., Nonlinear, Soft Matter Phys.*, 2015, **92**, 062311.
43 A. Pandey, P. B. S. Kumar and R. Adhikari, *Soft Matter*, 2016, **12**, 9068–9076.
44 M. S. D. Wykes, J. Palacci, T. Adachi, L. Ristroph, X. Zhong, M. D. Ward, J. Zhang and M. J. Shelley, *Soft Matter*, 2016, **12**, 4584–4589.
45 D. Saintillan, M. J. Shelley and A. Zidovska, *Proc. Natl. Acad. Sci. U. S. A.*, 2018, **115**, 11442–11447.

